ORIGINAL PAPER

A simplified methodology: pH sensing using an in situ fabricated Ir electrode under neutral conditions

Yuqi Chen[1,2] · Xiuting Li[1] · Danlei Li[2] · Christopher Batchelor-McAuley[2] · Richard G. Compton[2]

Abstract

Herein, a simplified fabrication method for the producing of a pH-sensitive iridium electrode is developed. The in situ electrochemical fabrication of an iridium oxide film is optimized and shown to be achievable under neutral conditions rather than the acidic conditions hitherto employed. The formation of a pH sensitive Ir(III/IV) hydrous film is confirmed via XPS. The amperometric pH-sensing properties of this electrochemically generated material were investigated using square wave voltammetry. In the pH range 2–13, the iridium oxide redox signal has a pH dependency of 86.1 ± 1.1 mV per pH unit for midpoint potentials with uncertainties being ± 0.01–0.05 pH. Finally, the newly developed pH sensor was used to measure the pH of a natural water sample with excellent results as compared to a conventional glass pH probe.

Introduction

The determination of pH quantifies how acidic or basic an aqueous solution is. It is probably the most commonly made measurement by a chemical sensor. Real-world examples of the importance of pH measurements abound. For example, the human body can be viewed as a large buffer solution with the blood pH being maintained within the near neutral range. Abnormally high blood pH (alkalosis), or abnormally low blood pH (acidosis) is used as an indicator of numerous health issues including Bartter (BS) and Gitelman (GS) syndromes and hyperlactatemia [1–3]. Alternatively in environmental applications, pH is directly linked to the solubility of heavy metals; the lower pH the more toxic the water possibly is as the metals tend to be more soluble [4]. In food chemistry, pH data reveals the fractionation, solubility and functional properties of essential nutrients [5].

IUPAC [6] defines pH as a function of the activity of the hydrogen ion in a solution:

$$pH = -\log a_{H^+} = -\log\left(\frac{m_{H^+}\gamma_{H^+}}{m^\theta}\right) \tag{1}$$

where a_{H^+} is the single ion activity (measured on the molality scale in mol kg^{-1}), γ_{H^+} is the activity coefficient of the hydrogen ion (H$^+$) at a molality of m_{H^+} and m^θ is the standard molality (1 mol kg^{-1}) [7]. Note that IUPAC chose to define the pH in terms of the single ion quantities despite it often being asserted that these are impossible to measure other than approximately [8, 9], although some ingenious work arounds have been proposed [10, 11]. In contrast, Rockwood has proposed an approach based on classical equilibrium thermodynamics and provides a clear historical summary of the debate [12].

To date, various methods, electrochemical and non-electrochemical, have been applied to measure pH values, summarised by Vonau and Guth [13]. The glass pH metre is ubiquitously used in the laboratory by applying direct potentiometric measurements. It is a rapid and convenient method for determining the activity of the hydrogen ion in a solution. However, there are errors affecting its use, most notably the alkaline/acid errors at too high or too low pH, dehydration of the electrode and a reliance on the accuracy of standard buffers [14]. Moreover, there is an essential need for regular, frequent and careful calibration, which must be referenced to a certified buffer solution. Note that the pH value and uncertainty of the reference buffer solution should also be determined using a calibrated measurement. Thus,

✉ Richard G. Compton
  Richard.compton@chem.ox.ac.uk

[1] Institute for Advanced Study, Shenzhen University, Shenzhen 518060, China
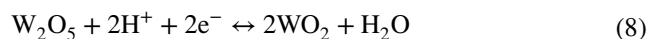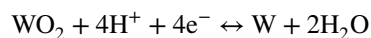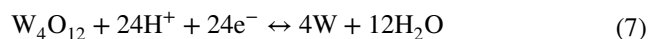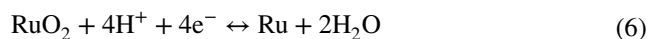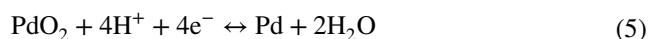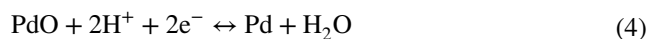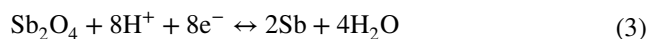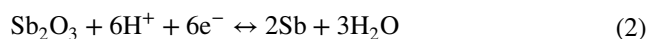
[2] Department of Chemistry, Physical and Theoretical Chemistry Laboratory, University of Oxford, South Parks Road, Oxford OX1 3QZ, UK

a traceability chain can be established relating a measured pH to the pH of a primary buffer solution, the basis and the historical development of which is described by Spitzer [15]. Alternatives to the glass electrode for potentiometric sensing have been suggested, for example by Inzelt [16, 17]. More generally, the use of potentiometric measurements however make precise and sensitive measurements challenging since the logarithmic relation between potential and activity results in a change of signal of a mere ca 60 mV per decade of concentration at 298 K. Apart from a glass electrode, electrode materials like carbon can be functionalised for pH sensing by various surface modifications, e.g. film formation and physical adsorption [18]. Electrodes can also be chemically modified with organic compounds or polymers, such as quinhydrone [19–23] and polypyrrole [24]. These provide an amperometric response which can be sensitive and selective to H$^+$ ions [19, 24–27]. One advantage of using amperometrically measured peak potentials is the scope for the doubling of sensitivity to 120 mV/decade through the use of two simultaneously immobilised pH-sensitive redox couples [28, 29]. A further merit of amperometric measurements is the ability to make calibration free pH measurements [30], while on the other hand, they are restricted to media containing some electrolyte.

Outside of electrochemistry, the fibre optic pH sensor is a non-electrochemical sensor with low cost and the ability for continuous sensing, which is commonly used in physiological studies [31–34]. Optical pH sensors usually consist of a pH indicator immobilised on an organic carrier. The indicator changes its chemical structure after interacting with H$^+$ ions, which leads to a variation of its optical response as a function of pH [35]. However, because the response of the colour change is sigmodal with pH, the accuracy is constrained and the useful detection range can be relatively narrow, often being 2–4 pH units only [36]. To be more specific, the optical pH sensors can be based on absorption [33], reflectance intensity [37] and fluorescence intensity [34, 38, 39]. The use of fluorescence is common due to its high sensitivity compared with reflectometric devices [39]. The short response time and scope for miniaturisation are further advantages. Notably, Optiz and Lubbers developed a fluorescence pH sensor that can measure the ionic strength and hydrogen ion activities simultaneously and continuously using hydroxypyrenetrisulfonic acid (HPTS) and β-methylumbelliferone [40]. Other indicators include 5- (and 6-) carboxynaphthofluorescein [39], and 7-hydroxycoumarin-3-carboxylic acid (HCC) [38] for pH measurements near-neutral values.

Metal/metal oxides or metal oxides pH sensors are widely studied especially in potentiometric mode based on the Nernst equation [41]. The potential determining reactions of some transition metal oxides MO$_x$ involves H$^+$ ions and the number of electrons transferred during the process and its

specific mechanism decide the E – pH relationship. pH sensitive metal/metal oxide systems M/MOx have been investigated including examples where M is antimony (Eqs. 2–3) [42–48], palladium (Eqs. 4–5) [43, 44, 49, 50], ruthenium (Eq. 6) [51–53] and tungsten (Eqs. 7–8) [54–56] and applied as pH sensors. The following are typical of the potential determining equilibria for typical M/MO$_x$ systems [54, 55]:

$$Sb_2O_3 + 6H^+ + 6e^- \leftrightarrow 2Sb + 3H_2O \tag{2}$$

$$Sb_2O_4 + 8H^+ + 8e^- \leftrightarrow 2Sb + 4H_2O \tag{3}$$

$$PdO + 2H^+ + 2e^- \leftrightarrow Pd + H_2O \tag{4}$$

$$PdO_2 + 4H^+ + 4e^- \leftrightarrow Pd + 2H_2O \tag{5}$$

$$RuO_2 + 4H^+ + 4e^- \leftrightarrow Ru + 2H_2O \tag{6}$$

$$W_4O_{12} + 24H^+ + 24e^- \leftrightarrow 4W + 12H_2O \tag{7}$$

$$WO_2 + 4H^+ + 4e^- \leftrightarrow W + 2H_2O$$

$$W_2O_5 + 2H^+ + 2e^- \leftrightarrow 2WO_2 + H_2O \tag{8}$$

While metal/metal oxide systems are commonly used in classical potentiometric mode in combination with a reference electrode to generate a potential reflecting the pH [44, 57–60], it is also possible to employ them in amperometric mode in which a pH sensitive voltammetric signal is used, the peak potential of which is used to indicate the pH [61–63]. One attraction of this approach is that the measurement generates a current–voltage plot the shape of which allows the assessment of the 'quality' of the measurement and hence the reliability of the data. This is particularly important under conditions where electrode fouling may occur, as in blood or other in vivo analysis [26, 64, 65], where in contrast to potentiometric measurements which simply deliver a number, amperometry/voltammetry allows the peak shape to provide an indication of the extent of for example electrode fouling or flag up a mis-functioning electrode [66]. One system where both potentiometry [44, 57, 67–70] and amperometry [26, 64] has been used in this way is the iridium/iridium oxide system.

The Ir/IrO$_x$ redox couple is one of the most popular candidates for pH sensors especially in aggressive environments such as high temperature and/or pressure [57, 67, 69, 71–74], which is also famous for its electrocatalytic behaviour for the O$_2$ and Cl$_2$ evolution reactions [75–79] and electrochromic properties of redox reactions [67, 71–73]. There are diverse methods for Ir oxide generation. Electrodeposition is one of the methods and uses a solution of potassium

hexachloroiridate(III) as a precursor [64, 80, 81]. The conditions and process required to form the final IrO_x are complex and hard to control, which lead to limited reproducibility [82–85]. Iridium oxides can also be prepared by sol–gel [86, 87] chemistry, sputtering [59, 88] or thermal methods [69, 85]. However, a pre-treatment, e.g. hydroxylation, is required prior to the usage of electrodes fabricated by the latter two approaches. This is because the resultant dry oxide films or anhydrous films are less hydrous than iridium oxide prepared electrochemically in an aqueous solution [64, 68, 89]. Meanwhile, sputtering is expensive, whereas the pH response of the thermally synthesised Ir electrode is highly dependent on the fabrication conditions [90].

It has been reported that the anodic iridium oxide film (AIROF) can be synthesised by cyclic voltammetry and the potential determining redox reaction happens within the iridium oxide film rather than on the Ir metal which simply serves as a conductive support [78, 79, 91–93]. Similar phenomena were also observed for Rh, Ru, Os and W [75, 94–97]. Based on this, in this paper, we develop a novel in situ AIROF fabrication methodology for pH sensing. Instead of employing ex situ potential cycling under acidic or basic conditions as previously explored [43, 67, 92, 93, 98, 99], neutral conditions were newly applied with AIROF being fabricated in situ so facilitating more remote and diverse pH measurements notably in medical and environmental applications. To further simplify the procedure, constant potential electrolysis (CPE) activation was applied and further optimised to mimic and replace CV activation, followed by square wave voltammetry (SWV) to obtain resultant the redox peaks used for pH measurement. The pH dependency of the redox peak position and scope of the method are studied in buffer solutions with different pH values. The methodology is applied to the pH measurement in authentic samples of pond water giving good agreement with pH values obtained independently by a classical commercial pH metre.

Experimental section

Chemicals and reagents

Solutions were prepared in ultra-pure water with a resistivity of 18.2 MΩ cm at 298 K (KMD-SHZ, CD Haochun Inc., China). All chemicals were of analytical grade and were used as received without any further purification. Buffer solutions were prepared using chemicals purchased from Shanghai Macklin Biochemical Co., Ltd.: citric acid (99.0%)/sodium citrate (99.5%) for the pH range 2.99–4.81, monopotassium phosphate (99.5%)/dipotassium phosphate (98.0%) for the pH range 5.99–8.00 and sodium carbonate (99.5%)/sodium bicarbonate (99.8%) for the pH range

9.02–9.85. To obtain pH = 1–2 solutions, hydrochloric acid (mass fraction = 36–38%, Guangzhou Chemical Reagent Factory, China) was diluted; for pH = 10.78–12.75, potassium hydroxide (95%, Shanghai Macklin Biochemical Co., Ltd.) was used. All solutions contained 100 mM KCl (99.0%, Sigma-Aldrich, China) as supporting electrolyte. The pH values of buffers were measured using a pH metre (SevenCompact. Mettler Toledo Instrument (Shanghai) Co., Ltd) calibrated using standard buffers of pH 4.01 ± 0.02, 7.00 ± 0.02 and 9.21 ± 0.02.

Electrochemical apparatus and methods

A high purity Ar flow was used to remove oxygen from all aqueous solutions prior to study. Electrochemical measurements were performed in a thermostatic (25 ± 1 °C) Faraday cage using a CHI760E Electrochemical Workstation (CH Instruments, Inc., Shanghai, China). A standard three electrode set up was used, consisting of a mercury/mercury sulphate/saturated K_2SO_4 solution reference electrode (MSE, + 0.64 V vs NHE at 25 °C, CH Instruments, Inc., China), a platinum wire counter electrode and an iridium electrode (0.1 mm in diameter, GoodFellow, UK) as the working electrode. An Ir electrode was pretreated by heating the metal using a flame gun using gas liquefied petroleum gas (butane ≥ 95%, Pan'an city Gas Co., Ltd., China) for 10 s to remove surface contamination and impurities. Cyclic voltammetry was used to study the electrochemical behaviour of the Ir electrode, while square wave voltammetry was conducted to determine the pH dependency of in situ modified Ir wire after constant potential electrolysis (CPE) activation.

XPS study and sample preparation

The four pure Ir wires (0.125 mm in diameter, Alfa Aesar (China) Chemicals Co., Ltd) were preflamed as discussed above. For three preflamed Ir wires, the potential cycling activation, starting at − 0.6 V vs MSE then scanning anodically to 0.45 V vs MSE and then cathodically to − 1.05 V vs MSE for 625 cycles was conducted in a degassed PBS solution (pH = 7.25). Then, the cyclic voltammetry was stopped at − 1.05 V, − 0.1 V or 0.3 V vs MSE, respectively, followed by application of the end potential for 60 s. The three Ir samples with electrochemical activation and the one without were sealed in separate vacuum tubes. The calibrated X-ray photoelectron spectroscopy (XPS, K-Alpha +) spectra are referenced to the C 1 s peak at 284.6 eV and were carried out for surface elemental analysis.

Real sample analysis

Pond water from Wenshan Lake located in Shenzhen University, China (113.93° E, 22.54° N), was used for the real

sample analysis. Prior to further analysis, natural water samples were filtered using filter paper (pore size 1 μm) to remove solid impurities. The KCl was then added to the natural water to realise a concentration of 100 mM.

Results and discussion

In the following sections, we first explore the oxidative voltammetry of iridium metal under conditions of near neutral pH to show the in situ formation of iridium oxide features which are subsequently used as the basis for amperometric pH sensing. XPS is used to confirm the inferred redox chemistry. Next, the in situ formation of iridium oxide under conditions of different fixed potentials is explored with the aim of permitting in situ sensor generation from an iridium electrode. This process is then optimised for the formation of pH sensitive iridium hydrous oxides. The pH response was further explored using square wave voltammetry (SWV) and an analytical methodology for pH defined in which the surface bound pH sensing redox couple is generated in situ from an iridium wire. Finally, the developed method was employed to determine the pH of a natural water sample.

Cyclic voltammetric study of Ir metal electro-oxidation

The formation of iridium oxides on the surface of an iridium wire was investigated voltammetrically. It was recognised that for reproducible data prior to a measurement, the surface of the Ir wire should be completely free of oxide which is commonly found on such surfaces. For some electrode

materials, it is possible to remove such traces of oxide electrochemically but this is known to be unreliable for iridium, leaving a small amount of hydrous oxide on the surface [92, 100, 101]. For this reason, prior to voltammetry, Ir surfaces were treated by pre-flaming in the present work to renew the surface of the metal electrode between each experiment. The effects of pre-flaming are shown in Sect. 1 of SI where a clear memory effect for an electrode without preflaming was observed, whereas the cyclic voltammograms are reproducible when using a preflamed electrode.

To explore the electrochemical behaviour of an Ir wire in neutral solution, the pre-flamed Ir electrode was immersed in a degassed phosphate buffer solution (PBS) with 0.1 M KCl (pH = 7.25) and cyclic voltammetry was conducted for 625 cycles starting at a potential of − 0.6 V with scan reversal at a potential of 0.45 to − 1.05 V vs MSE where the potential again reversed as shown in Fig. 1a. The figure shows four voltammetric features labelled A, B, C and D. Feature A is assigned to the underpotential adsorption of hydrogen (H_{upd}) [102, 103].

$$M(s) + H_3O^+ + e^- \rightleftharpoons M - H_{ad} + H_2O \rightleftharpoons \frac{1}{2}H_2 + M - H_2O_{ad}$$
(9)
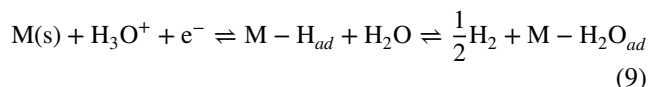
In contrast to feature A, features B and C steadily increase with increasing scan number. This voltammetric response is markedly different from that observed for platinum [104]. Here, feature B is attributed to the Ir (III)–Ir (IV) redox transition with formation of hydrous oxides. This process has been reported to involve various possible redox reactions between the reduced and oxidised forms of oxyhydroxide where the exact stoichiometric composition of the hydrous film is reported as hard to determine [64,
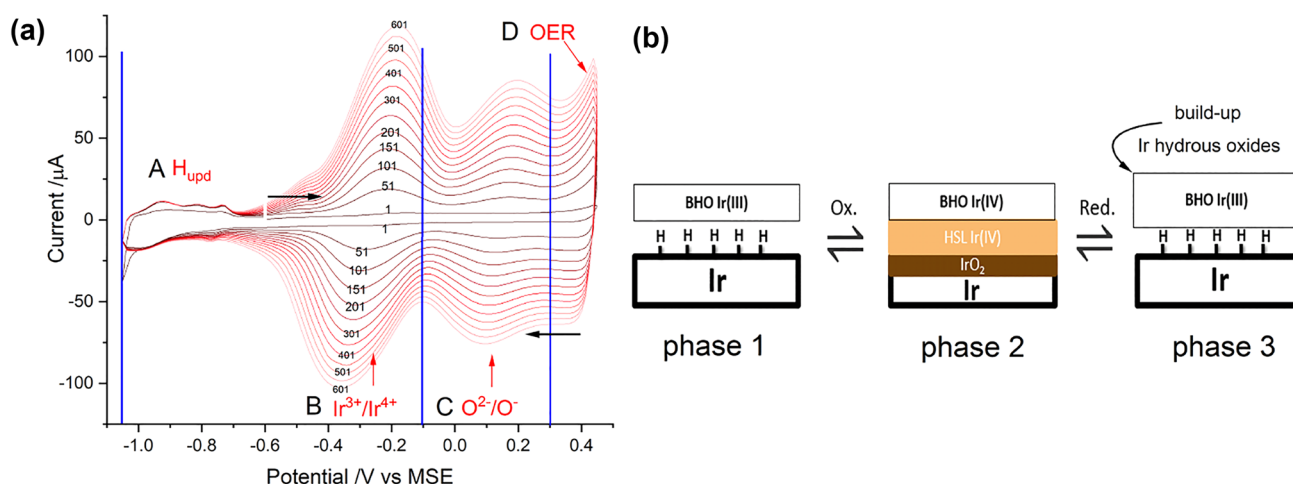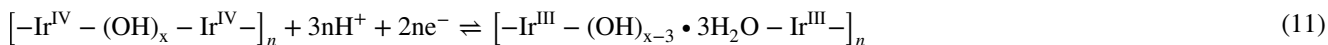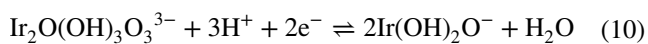

Fig. 1 (a) Cyclic voltammograms in a degassed buffer solution with pH = 7.25 showing the activation of an Ir wire at a scan rate of 0.5 V s⁻¹ for multiple cycles. The start potential was − 0.6 V vs MSE. The blue lines show the potentials used for constant potential oxide generation (see text). (b) Schematic mechanism of Ir electrode activation. BHO, bulk hydrous oxide; HSL, hydrated surface layer [92]

67, 105]. The equilibria suggested by Olthuis et al. [67] and Burke et al. [105] are as follows:

$$Ir_2O(OH)_3O_3{}^{3-} + 3H^+ + 2e^- \rightleftharpoons 2Ir(OH)_2O^- + H_2O \quad (10)$$

$$\left[-Ir^{IV} - (OH)_x - Ir^{IV}-\right]_n + 3nH^+ + 2ne^- \rightleftharpoons \left[-Ir^{III} - (OH)_{x-3} \bullet 3H_2O - Ir^{III}-\right]_n \quad (11)$$

The equilibria in (10) and (11) suggest a super-Nernstian pH dependency of ca 89 mV per pH unit, reflecting the fact the relative numbers of electrons and protons consumed in reaction (10) and (11) [57, 64, 106].

There are different interpretations of feature C. Pickup and Birss suggested that it corresponds to further oxidation of the Ir hydrous oxides, e.g. from Ir (IV) to Ir (VI) [92]. However, later reports from Pfeifer et al. [78, 79, 91] proposed assigning it to the oxidation of the oxide anion O^{2-}, contained in the IrO_x matrix in form of adsorbed OH groups, to O^-:

$$IrO_xO^{II-}H \rightleftharpoons IrO_xO^{I-} + H^+ + e^- \quad (12)$$
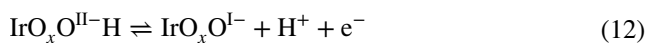
Feature D is related to the oxygen evolution reaction (OER):

$$2H_2O \rightarrow O_2 + 4H^+ + 4e^- \quad (13)$$

It has been suggested that the IrO_xO^{I-} formed during the redox reaction in feature C is the catalyst for OER where Eq. (14) explains its possible electrocatalytic behaviour explicitly [79]:

$$IrO_xO^{I-} + H_2O \rightarrow IrO_xO^{I-} - O^{I-} - H + H^+ + e^- \rightarrow IrO_x + O_2 + 2H^+ + 3e^- \quad (14)$$
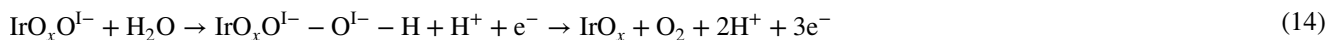
Based on the literature, it is possible to summarise the likely sequence of events underpinning the voltammetry shown in Fig. 1. Initially during the first sweep of potential cycling, the pure Ir is oxidised to IrO_2 by potentials ranging from -0.65 to 0.15 V vs MSE and its surface immediately becomes hydrated when an anodic potential is applied. The resulting Ir (IV) hydrous oxide can subsequently only be reduced back to Ir (III) in contrast to IrO_2 with the applied potential negative than approximate -1.05 V which is thought to be capable of being reduced to pure Ir when the cyclic voltammetry is swept cathodically [92].

Figure 1b schematically shows the state of the surface of the iridium electrode at different stages of the voltammetry and seeks to explain the build-up of the features B and C from one potential cycle to the next. In Fig. 1b, phase 1 shows a pure Ir wire with bulk Ir(III) hydrous oxide (BHO Ir(III)) accumulated from previous scans on its surface. When an anodic potential is applied

(between -0.65 and 0.15 V vs MSE), the Ir metal is again partly oxidised to IrO_2 and the previously formed BHO Ir(III) is oxidised to form BHO Ir(IV). Note that the Ir (IV) hydrated surface layer (HSL Ir (IV)) shown at phase 2 differs from BHO Ir(IV) formed in previous cycles in that it is newly formed and bonded to the inner IrO_2 layer. Then, by applying a cathodic potential at approximately -1.05 V vs MSE, neither the BHO nor the HSL Ir (IV) can be reduced to oxidation states lower than Ir (III). As a result, a new layer of BHO Ir (III) from HSL Ir (IV) is added to the original Ir metal surface as shown in phase 3. Consequently, as the number of potential cycling increases as shown in Fig. 1, a progressive build-up of the Ir hydrous oxide layer was observed with scans due to the repeated redox process mentioned above. Referring to the cyclic voltammogram in Fig. 1a, the thickness of accumulated Ir hydrous oxide after 625 cycles is estimated to be around 0.46 μm, assuming that the H_{upd} represents a monolayer (Sect. 2 of SI).

To confirm the proposed interpretation and analyse the formed Ir hydrous oxide layer, three surfaces were electrochemically generated for XPS with a pure Ir wire surface cleaned by flaming for comparison. Figure SI. 3 shows the resulting (a) Ir 4f and (b) O 1 s XPS spectra and Table 1 states the details of the spectra, which are consistent with the proposed mechanism above and to be more specific, the formed thick layer is iridium (III/IV) hydrous oxide as a result of potential cycling. The presence of this even when the sample for spectroscopic evaluation being withdrawn at -1.05 V indicates the chemical irreversibility of the formation of this layer (see detailed discussion in Sect. 3 of SI).

In a conclusion, an Ir wire can be activated under neutral rather than acid conditions forming a hydrous iridium (III/IV) oxide layer, which is pH-sensitive. In the following, we use this approach to develop a pH sensor based on the in situ activation of an Ir electrode under neutral pH conditions.

Optimisation of the electrode activation

In this sub-section, the most effective potential window of potential cycling for the growth of Ir hydrous oxide was first studied based on the conclusions of the last section. Next constant potential oxidation was optimised to mimic the cyclic voltammetry by applying various fixed potentials for defined periods of time to develop a method of in situ

generation of the pH sensitive Ir hydrous oxide. Square wave voltammetry (SWV) was then conducted to record the redox peaks of the resulting modified Ir surfaces under different pH conditions and an analytical methodology developed.

Optimisation of the potential window for the growth of pH-sensitive iridium hydrous oxide

The formation mechanism of the Ir hydrous oxide layers was clarified in the previous section. Next, the potential window of cycling was optimised to improve the sensitivity in respect of pH detection. As shown in Fig. 2a, cyclic voltammetry of a pre-flamed Ir wire with different potential windows were conducted in a degassed PBS solution with 0.1 M KCl (pH = 7.25) at 0.5 V s^{-1}. The CV starts at a potential of −0.6 V and first swept anodically to a fixed potential of 0.45 V and the swept to different cathodic limits varies from −1.05 to −0.7 V vs MSE. The 10th cycle is displayed in Fig. 2a to find the optimised cathodic potential. Figure 2b shows the 10th cyclic voltammograms with the cathodic potential being fixed at −1.05 V and the anodic potential was progressively increased to 0.5 V from 0.2 V vs MSE.

The resultant Ir (III/IV) redox couple in Fig. 2a becomes better defined with a high signal to background level with a reductive limit of −1.05 V while in Fig. 2b, the redox couple of the 10th cycle becomes better-defined when the positive potential limit is extended to 0.45 V. Extending the limits beyond −1.05 V or +0.45 V showed no further improvement in the quality of the signal, which is consistent with literature [92, 107]. Pickup and Birss also suggested that the hydrous oxide begins to dissolve when more positive potentials were applied [92]. From our measurement, it is clear that

the potentials between 0.2 and 0.45 V has greater influence on the formation of the Ir hydrous oxide, while extension of the cathodic limit increases the rate of growth only slightly. An explanation for this may be that the completion of redox transition between O$^{2-/-}$ contained in the IrO$_x$ matrix in form of adsorbed OH groups (feature C) is a prerequisite of hydrous oxide formation.

To summarise, for the growth of hydrous oxide, the potential window must embrace both the upper critical limit and the lower critical limit, to be more specific, anodically to 0.45 V and cathodically to − 1.05 V vs MSE. One can also conclude that during cyclic voltammetry, only around 20% of the experimental potential scan while the electrode is at extreme potentials actually induces the chemistry for the growth of hydrous oxide. This latter observation encourages seeking a simpler activation method using constant potential electrolysis as below.

Optimisation of constant potential electrolysis for in situ Ir hydrous oxide growth

Different potential sequences were developed with time-scales dictated by the observation that potential cycling between − 1.05 and 0.45 V for 10 cycles was effective to obtain a clear redox couple suggesting that around 12 s might be needed at each potential limit to demonstrate a comparable effect as the potential cycling. Thus, three CPE methods were analysed. Figure 3a–c are the plots of potentials against time to demonstrate the three CPE activations to mimic and enhance the potential cycling activation established as above. For method 1 in Fig. 3a, a potential of 0.45 V was applied for 12 s and followed by a potential of −1.05 V for 12 s. Method 2 has the same total activation
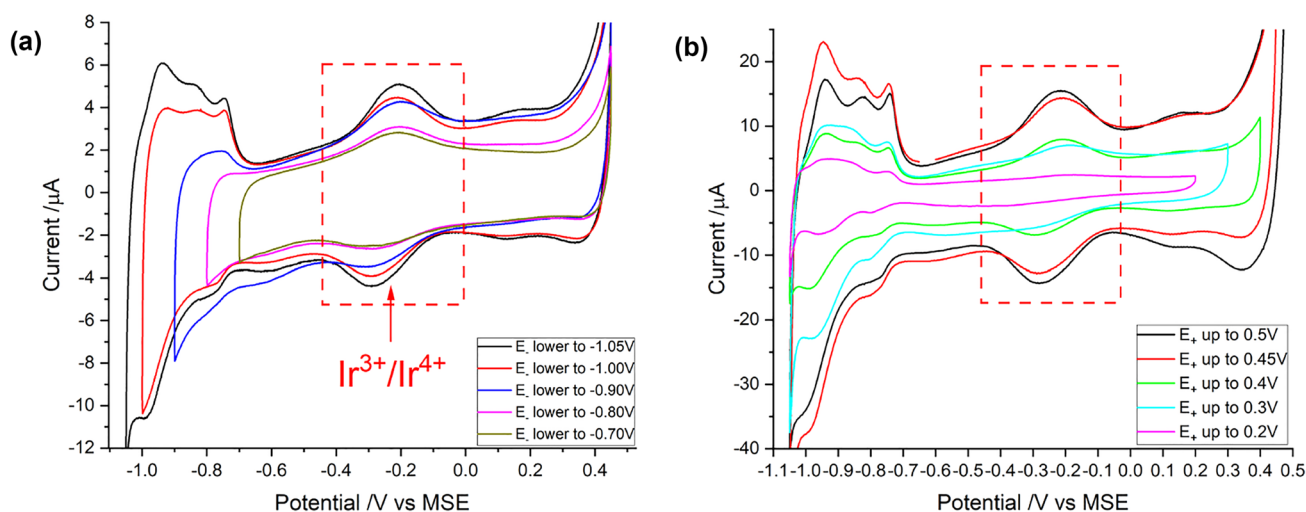

Fig. 2 Cyclic voltammograms of the 10th cycle in degassed buffer solution with pH = 7.25 starting at a potential of − 0.6 V for activation of Ir wire with different (a) cathodic and (b) anodic potentials at a scan rate of 0.5 Vs^{-1}

time at each limit potential but was divided into six repeats of potential so that 2 s was spent on each potential on every repeat (Fig. 3b). As shown in Fig. 3c, method 3 is a CPE method with four repeats of potential switch (2 s for each potential segment) for a shorter overall duration (16 s rather than 24 s).

Figure 3d shows the three cyclic voltammograms resulting from the three activation methods and, as expected, display the presence of two redox couples ($Ir^{3+/4+}$ and $O^{2-/-}$) as characterised above with formal potentials of ca. -0.26 V and 0.13 V vs MSE, respectively. Comparison of the three voltammograms shows that method 1 produces a much weaker signal than methods 2 and 3 but that there is a negligible difference between the later.

We conclude that CPE is effective for the growth of Ir hydrous oxide films and that method 3 is suitable. Hence, CPE with four repeats of potential switch between 0.45

and -1.05 V vs MSE will be used as the in situ Ir electrode fabrication method for further study as reported below.

pH dependency of the iridium hydrous oxide layer in buffer solutions

In this section, the pH dependency of the iridium hydrous oxide layer is investigated by square wave voltammetry (SWV) using an Ir wire activated by the CPE method established as above. The optimisation of SWV parameters, including frequency, step potential and amplitude, in a degassed PBS solution with 0.1 M KCl (pH = 7.25) was implemented to obtain the best-defined square wave voltammograms for pH measurements (Sect. 4 of SI). The optimised SWV with frequency of 90 Hz, amplitude of 60 mV and step potential of 1 mV were applied for pH measurements in buffer solutions with various pHs. Prior
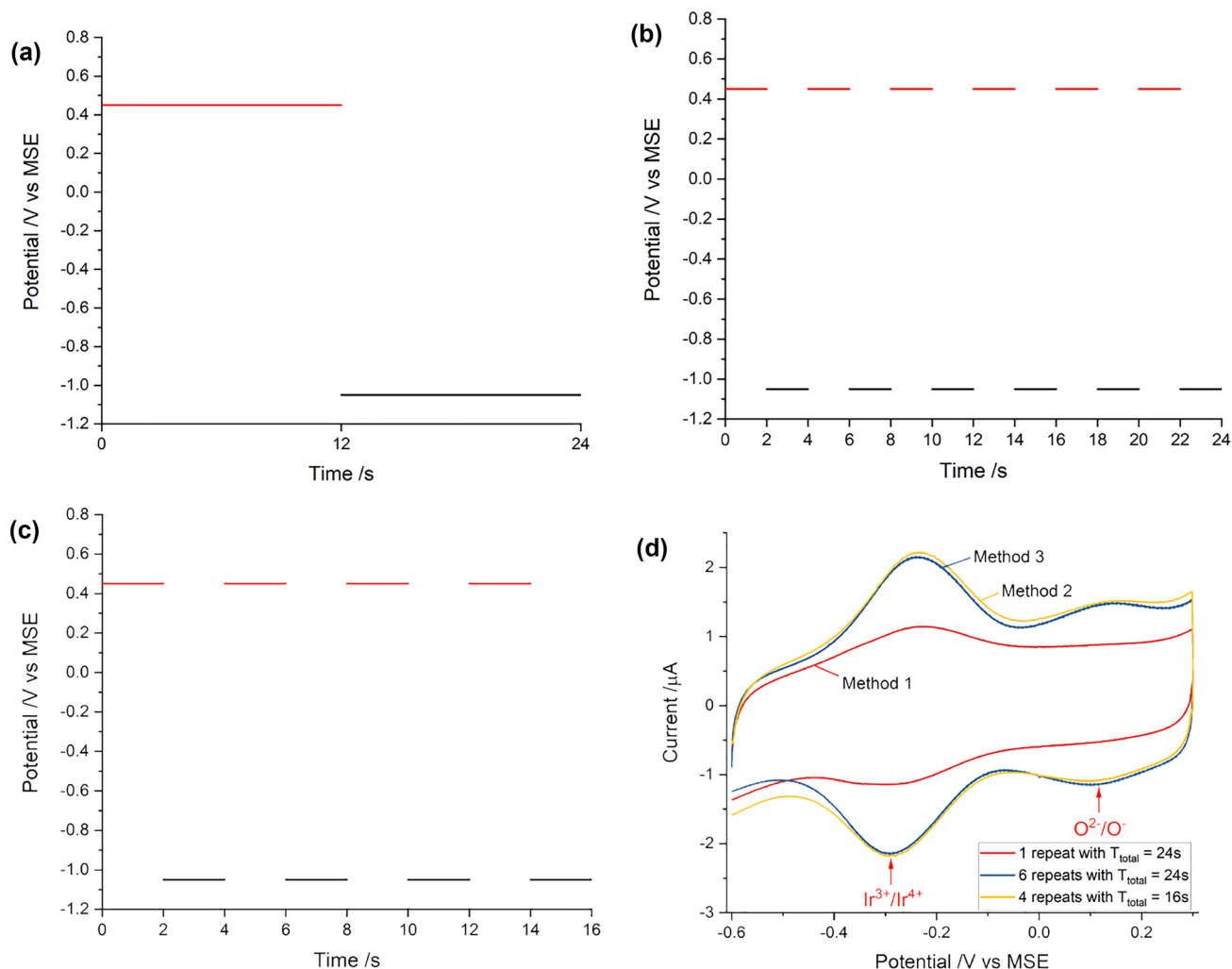

Fig. 3 CA activation with switch of potentials at 0.45 V and -1.05 V vs MSE (a) for one time with 12 s at each potential, (b) for six times with 2 s at each potential and (c) for four times with 2 s at each potential; (d) resultant cyclic voltammograms of the 10th cycle after CA activation in degassed buffer solution with pH = 7.25 at a scan rate of 0.1 V s^{-1}

to the measurements, the pHs of buffers were measured by a pH metre, with an uncertainty of 0.01 (x-axis error-bar in Fig. 4c). SWV were first scanned anodically to obtain a net oxidative peak and then scans were immediately reversed to obtain a desired reduction peak (Fig. 4a and b). The expected Ir(III/IV) SWV peaks were observed in the potential range within ca 0.11 to − 0.73 V for scans in both directions for pH = 2–13, while for pH = 2–5, a small peak was seen during the oxidation scan, with peak potentials being about 0.32 V more negative than that of the target oxidation peak. But the pre-peak was deemed not to interfere with the measurements of the main peak to be used for the pH determination. For pH values lower than 2 (Sect. 5 of SI), three peaks were observed during oxidation scans, notably, at ca − 0.12 V, 0.09 V and 0.31 V for pH = 1.15 and − 0.11 V, 0.06 V and 0.22 V vs MSE for pH = 1.86 (Fig. S5a). The reduction signals were broad for both pH values, and this was attributed to the overlap of 2 peaks (see Fig. S5b). Given the voltammetric complexity seen at

low pH, it was decided to focus on the pH range from 2.0 to 13.0 for establishing a measurement protocol.

The analytically useful (for pH measurement) Ir(III/IV) redox couple obtained in solutions with pH = 2–13 showed a shift in the peak potentials towards more negative potentials as the pH increased for both oxidative and reductive scans. To analyse the data, the oxidation/reduction peak potentials and midpoint potential of the in situ fabricated iridium oxide electrode were all recorded. The plots of potentials against pH as measured from pH metre are shown in Fig. 4c. The gradients of the slopes were 85.6 ± 2.3, 90.0 ± 2.1 and 86.1 ± 1.1 mV per pH unit for oxidation/reduction peak potentials and midpoint potential, respectively. The pH dependency is above the ca 60 mV per pH unit response of a classical glass electrode but consistent with the equilibria proposed by Olthuis et al. [67] and Burke et al. [105] being around 89 mV per pH unit as given in Eqs. 9 and 10 above where three protons are transferred per two electrons. The higher response
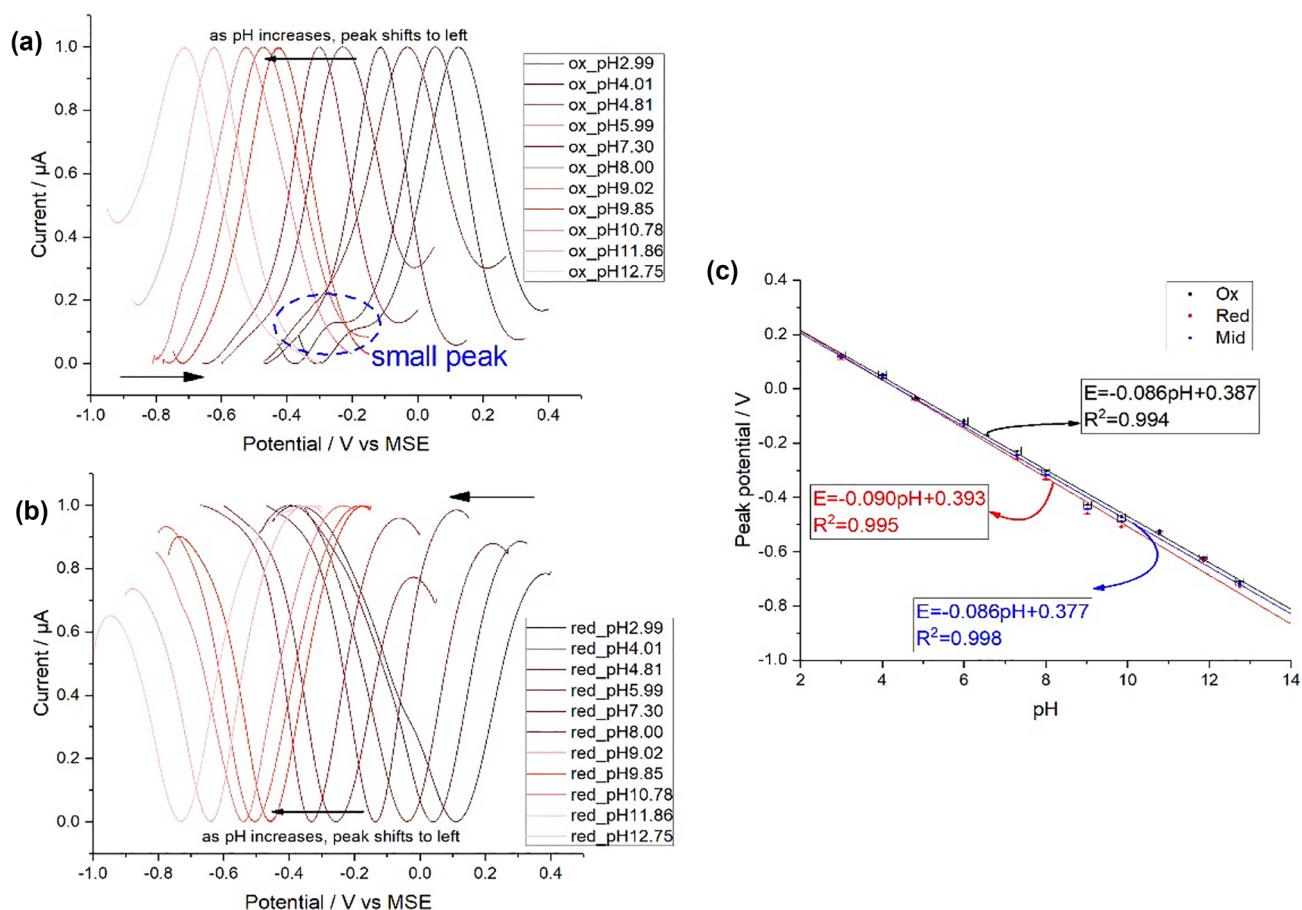

Fig. 4 Normalised square wave voltammetry (frequency 75 Hz, step potential 1 mV and amplitude 60 mV) response of iridium hydrous oxide on iridium wire electrode with varying pH of different buffers ranging from 2.99 to 12.75 (**a**) oxidation and (**b**) reduction. (**c**) Plots of potentials against pH value reading from pH metre (black dots: oxidation, red dots: reduction and blue dots: mid-point potential)

per pH unit is a clear merit of the iridium oxide approach to pH sensing.

For the uncertainty of pH measurement, bootstrap was used [108]. Each of these simulated pH values by boot-strap has its own values of mean and uncertainty (Table 2, Sect. 6 of SI). Oxidation peaks and midpoints have standard deviations smaller that of reduction peaks (0.2 to 0.7), while midpoints are considered to be the reference for the later application, with pH uncertainties ranging from 0.1 to 0.5.

Real sample analysis: pH measurement in natural water

The pH dependency of the in situ fabricated iridium hydrous oxide layer on the iridium wire in buffer solutions was obtained and investigated in the previous section using CPE activation method followed by SWV to improve signal-to-background ratio of the redox peak of interest. This electrode was subsequently employed for pH sensing of a natural water sample (Wenshan Lake located in Shenzhen University, China) to investigate the capability of the use under real world conditions.

First, the iridium wire was activated using CPE with 4 repeats of potentials which switched between 0.45 and − 1.05 V vs MSE in a PBS solution with 0.1 M KCl (pH = 6.91). Then, SWV with the step potential of 1 mV, amplitude of 60 mV and frequency of 90 Hz was conducted in the pond water containing 0.1 M KCl. The effect of 0.1 M KCl as supporting electrolytes in pond water on the pH measurement using an Ir wire is demonstrated in Sect. 7 of SI. The oxidation peaks were recorded using
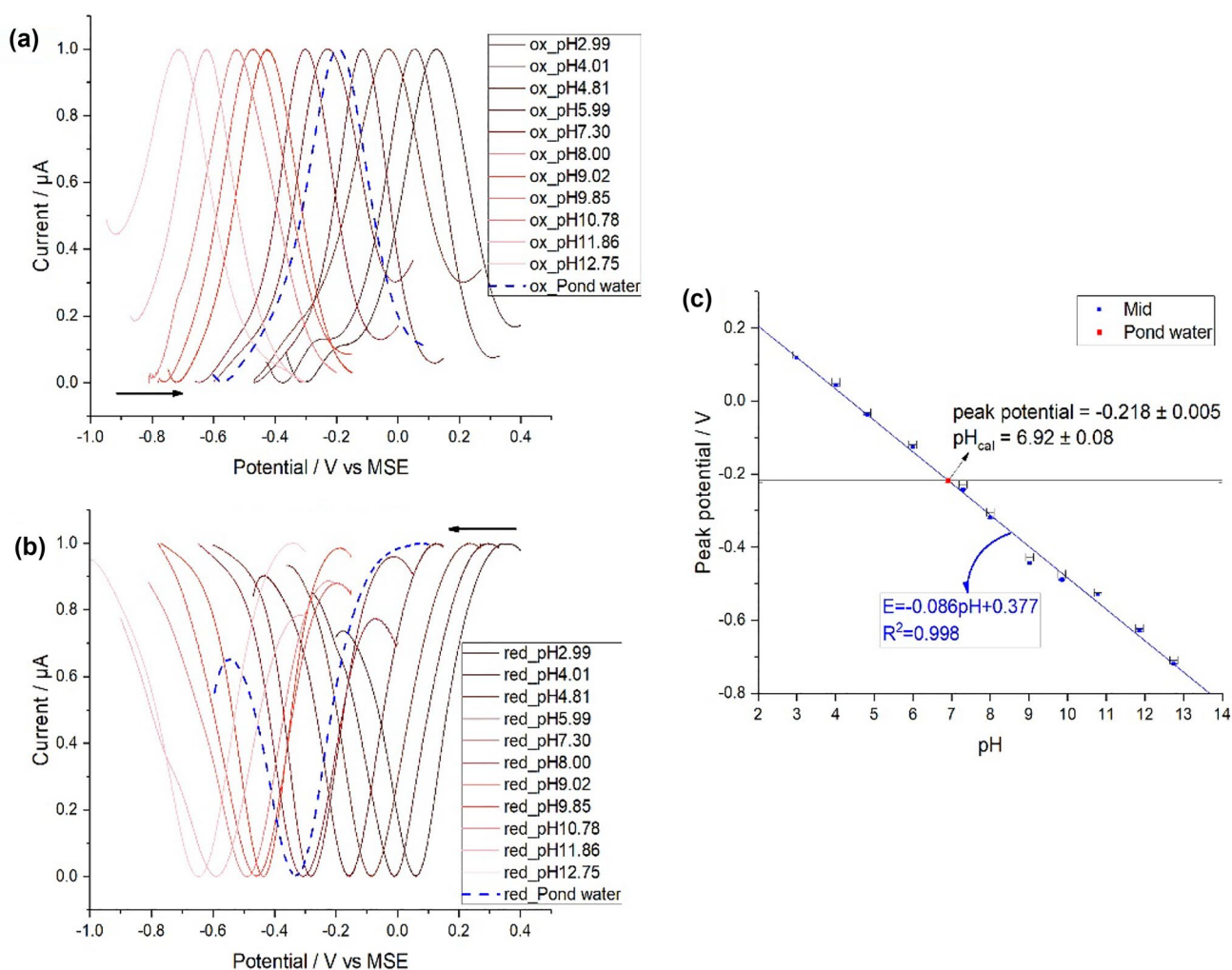

Fig. 5 Overlaid square wave voltammetry (frequency 75 Hz, step potential 1 mV and amplitude 60 mV) response of iridium hydrous oxide on an iridium wire in degassed pond water after CPE activation in PBS solution with the same pH = 6.91 (**a**) oxidation and (**b**) reduction. (**c**) Overlaid average mid-point potential obtained in pond water with the plots of potentials against pH value reading from pH metre from previous section (red dot: pond water and blue dots: mid-point potential obtained previously)

SWV which initially swept to positive potentials and the scans were then reversed to obtain reduction peaks (blue dashed lines in Fig. 5a and b). The redox peaks obtained in the natural water samples were overlaid with previous results (solid lines). Three repeat experiments were done for an improved accuracy of the measurements; the average Ir(III/IV) oxidation peak from SWV is at -0.195 ± 0.005 V and reduction peak is at -0.241 ± 0.007 V with a corresponding average mid-point potential of -0.218 ± 0.005 V vs MSE. The pH value of the pond water sample was then calculated to be 6.92 ± 0.08 by adapting the pH dependency obtained in buffer solutions (blue dots in Fig. 5c). The reliability and accuracy for pH sensing in pond water using such iridium electrode have been proved by comparing the calculated pH value (6.92 ± 0.08) and the value measured by a commercial pH metre (6.91 ± 0.01). Thus, one can conclude that this in situ fabricated Ir wire is an ideal pH sensor under neutral condition.

Conclusions

In this work, the fabrication and performance of an iridium oxide electrode was studied. First, the cyclic voltammetry combined with XPS study demonstrated that an Ir wire can be activated under neutral rather than acid or basic conditions and the pH sensitivity of the formed hydrous iridium oxide layer is controlled by the Ir (III/IV) couple at all potentials used for pH measurement. Cyclic voltammetry was used to identify the potentials required to form the pH sensitive layers allowing a significant simplification of the formation by using constant potential electrolysis (CPE) with four repeats of potential switch between 0.45 and -1.05 V vs MSE rather than potential cycling. Then, the pH dependency of the electrode was studied in buffer solutions employing square wave voltammetry. The detection limit is pH = 2–13 and the gradients of the slopes being 85.6 ± 2.3, 90.0 ± 2.1 and 86.1 ± 1.1 mV per pH unit for oxidation/reduction peak potentials and mid-point potentials, respectively. Uncertainties of pH measurement are ± 0.01–0.05 pH units for midpoint potential. Finally, the measured pH of a natural water sample using the Ir electrode is 6.92 ± 0.08, while that obtained by a pH metre is 6.91 ± 0.01. The insignificant difference proves that this in situ fabricated Ir wire is an ideal pH sensor for use under neutral conditions and where in situ generation is advantageous.

References

1. Kellum JA (2000) Determinants of blood pH in health and disease. Crit Care 4:6. https://doi.org/10.1186/cc644
2. Galla JH (2000) Metabolic alkalosis. J Am Soc Nephrol 11:369–375. https://doi.org/10.1681/asn.v112369
3. Mizock BA, Falk J (1992) Lactic acidosis in critical illness. Crit Care Med 20:80–93
4. Michaud JP (1991) A citizien's guide to understanding and monitoring lakes and streams. Envirovision-Environmental Consulting Service, Washington, USA
5. Ragab DM, Babiker EE, Eltinay AH (2004) Fractionation, solubility and functional properties of cowpea (Vigna unguiculata) proteins as affected by pH and/or salt concentration. Food Chem 84:207–212. https://doi.org/10.1016/S0308-8146(03)00203-6
6. Mills I, Cvitaš T, Homann K, Kallay N, Kuchitsu K (1993) Quantities, units and symbols in physical chemistry. Oxford; Boston: Blackwell Science; Boca Raton, Fla.: CRC Press [distributor]
7. Buck R, Rondinini S, Covington A, Baucke F, Brett CM, Camoes M, Milton M, Mussini T, Naumann R, Pratt K (2002) Measurement of pH. Definition, standards, and procedures (IUPAC Recommendations 2002). Pure Appl Chem 74:2169–2200. https://doi.org/10.1351/pac200274112169
8. Malatesta F (2000) The impossibility of measuring individual ion activity coefficients using ion selective electrodes. J Solution Chem 29:771–779. https://doi.org/10.1152/jappl.1976.40.4.64410.1023/A:1005137929282
9. Rieger PH (1987) Electrochemistry. Prentice Hall, United States
10. Shibata M, Kato M, Iwamoto Y, Nomura S, Kakiuchi T (2013) Potentiometric determination of pH values of dilute sulfuric acid solutions with glass combination electrode equipped with ionic liquid salt bridge. J Electroanal Chem 705:81–85. https://doi.org/10.1016/j.jelechem.2013.07.024
11. Shibata M, Sakaida H, Kakiuchi T (2011) Determination of the activity of hydrogen ions in dilute sulfuric acids by use of an ionic liquid salt bridge sandwiched by two hydrogen electrodes. Anal Chem 83:164–168. https://doi.org/10.1021/ac1021216
12. Rockwood AL (2015) Meaning and measurability of single-ion activities, the thermodynamic foundations of pH, and the Gibbs free energy for the transfer of ions between dissimilar materials. Chemphyschem : Eur J Chem Phys Phys Chem 16:1978–1991. https://doi.org/10.1002/cphc.201500044
13. Vonau W, Guth U (2006) pH monitoring: a review. J Solid State Electrochem 10:746–752. https://doi.org/10.1007/s10008-020-04647-6
14. Skoog DA, West DM, Holler FJ, Crouch SR (2013) Fundamentals of analytical chemistry. Cengage learning, USA
15. Spitzer P, Pratt KW (2011) The history and development of a rigorous metrological basis for pH measurements. J

Solid State Electrochem 15:69–76. https://doi.org/10.1007/s10008-010-1106-9

16. Borsos K, Inzelt G (2016) A new electrode for acid-base titration based on poly (copper phthalocyanine). J Solid State Electrochem 20:1215–1222. https://doi.org/10.1007/s10008-015-2899-3

17. Inzelt G, Borsos K (2015) Replacement of the glass electrode by graphite at acid-base potentiometric titrations. Stud Univ Babes-Bolyai, Chem 60:23–30

18. Kahlert H (2008) Functionalized carbon electrodes for pH determination. J Solid State Electrochem 12:1255–1266. https://doi.org/10.1007/s10008-008-0566-7

19. Aquino-Binag C, Pigram PJ, Lamb RN, Alexander PW (1994) Surface studies of quinhydrone pH sensors. Anal Chim Acta 291:65–73. https://doi.org/10.1016/0003-2670(94)85127-1

20. Leventis HC, Streeter I, Wildgoose GG, Lawrence NS, Jiang L, Jones TGJ, Compton RG (2004) Derivatised carbon powder electrodes: reagentless pH sensors. Talanta 63:1039–1051. https://doi.org/10.1016/j.talanta.2004.01.017

21. Wildgoose GG, Pandurangappa M, Lawrence NS, Jiang L, Jones TGJ, Compton RG (2003) Anthraquinone-derivatised carbon powder: reagentless voltammetric pH electrodes. Talanta 60:887–893. https://doi.org/10.1016/S0039-9140(03)00150-4

22. Wildgoose GG, Leventis HC, Streeter I, Lawrence NS, Wilkins SJ, Jiang L, Jones TG, Compton RG (2004) Abrasively immobilised multiwalled carbon nanotube agglomerates: a novel electrode material approach for the analytical sensing of pH. ChemPhysChem 5:669–677. https://doi.org/10.1002/cphc.200400030

23. Scholz F, Düssel H, Meyer B (1993) A new pH-sensor based on quinhydrone. Fresenius' journal of analytical chemistry 347:458–459. https://doi.org/10.1007/bf00635475

24. Hailin G, Yucheng L (1994) Characterization of a chemoresistor pH sensor based on conducting polypyrrole. Sens Actuators, B Chem 21:57–63. https://doi.org/10.1016/0925-4005(94)01228-8

25. LeBlanc O, Brown J Jr, Klebe J, Niedrach L, Slusarczuk G, Stoddard W Jr (1976) Polymer membrane sensors for continuous intravascular monitoring of blood pH. J Appl Physiol 40:644–647. https://doi.org/10.1152/jappl.1976.40.4.644

26. Chaisiwamongkhol K, Batchelor-Mcauley C, Compton RG (2017) Amperometric micro pH measurements in oxygenated saliva. Analyst 142:2828–2835. https://doi.org/10.1039/c7an00809k

27. Makos MA, Omiatek DM, Ewing AG, Heien ML (2010) Development and characterization of a voltammetric carbon-fiber microelectrode pH sensor. Langmuir 26:10386–10391. https://doi.org/10.1152/jappl.1976.40.4.64410.1021/la100134r

28. Streeter I, Leventis HC, Wildgoose GG, Pandurangappa M, Lawrence NS, Jiang L, Jones TG, Compton RG (2004) A sensitive reagentless pH probe with a ca. 120 mV/pH unit response. J Solid State Electrochem 8:718–721. https://doi.org/10.1007/s10008-004-0536-7

29. Lawrence NS, Pagels M, Hackett SF, McCormack S, Meredith A, Jones TG, Wildgoose GG, Compton RG, Jiang L (2007) Triple component carbon epoxy pH probe. Electroanalysis: Int J Dev Fund Pract Asp Electroanalysis 19:424–428. https://doi.org/10.1002/elan.200603725

30. Xiong L, Batchelor-McAuley C, Compton RG (2011) Calibrationless pH sensors based on nitrosophenyl and ferrocenyl co-modified screen printed electrodes. Sens Actuators, B Chem 159:251–255. https://doi.org/10.1016/j.snb.2011.06.082

31. Gu B, Yin M-J, Zhang AP, Qian J-W, He S (2009) Low-cost high-performance fiber-optic pH sensor based on thin-core fiber modal interferometer. Opt Express 17:22296–22302. https://doi.org/10.1364/OE.17.022296

32. Gupta BD, Sharma S (1998) A long-range fiber optic pH sensor prepared by dye doped sol-gel immobilization technique. Optics Communications 154:282–284. https://doi.org/10.1016/S0030-4018(98)00321-6

33. Peterson JI, Goldstein SR, Fitzgerald RV, Buckhold DK (1980) Fiber optic pH probe for physiological use. Anal Chem 52:864–869. https://doi.org/10.1021/ac50056a022

34. Munkholm C, Walt DR, Milanovich FP, Klainer SM (1986) Polymer modification of fiber optic chemical sensors as a method of enhancing fluorescence signal for pH measurement. Anal Chem 58:1427–1430. https://doi.org/10.1021/ac00298a034

35. Zhang J, Zhou L (2018) Preparation and optimization of optical pH sensor based on sol-gel. Sensors (Basel, Switzerland) 18:3195. https://doi.org/10.3390/s18103195

36. Suah FBM, Ahmad M, Taib MN (2003) Applications of artificial neural network on signal processing of optical fibre pH sensor based on bromophenol blue doped with sol–gel film. Sens Actuators, B Chem 90:182–188. https://doi.org/10.1016/S0925-4005(03)00026-1

37. Sotomayor PT, Raimundo IM Jr, Zarbin AJ, Rohwedder JJ, Neto GO, Alves OL (2001) Construction and evaluation of an optical pH sensor based on polyaniline–porous Vycor glass nanocomposite. Sens Actuators, B Chem 74:157–162. https://doi.org/10.1016/S0925-4005(00)00726-7

38. Offenbacher H, Wolfbeis OS, Fürlinger E (1986) Fluorescence optical sensors for continuous determination of near-neutral pH values. Sensors and Actuators 9:73–84. https://doi.org/10.1016/0250-6874(86)80008-7

39. Wolfbeis OS, Rodriguez NV, Werner T (1992) LED-compatible fluorosensor for measurement of near-neutral pH values. Microchim Acta 108:133–141. https://doi.org/10.1007/BF01242422

40. Opitz N, Lübbers DW (1983) New fluorescence photometrical techniques for simultaneous and continuous measurements of ionic strength and hydrogen ion activities. Sensors and Actuators 4:473–479. https://doi.org/10.1016/0250-6874(83)85059-8

41. Feiner A, McEvoy A (1994) The nernst equation. J Chem Educ 71:493. https://doi.org/10.1021/ed071p493

42. Vonau W, Decker M, Enseleit U, Gerlach F (2020) Is there still a need for the antimony electrode 100 years after its introduction as a pH sensor? J Solid State Electrochem 24:3269–3277. https://doi.org/10.1007/s10008-020-04647-6

43. Głab S, Hulanicki A, Edwall G, Ingman F (1989) Metal-metal oxide and metal oxide electrodes as pH sensors. Crit Rev Anal Chem 21:29–47. https://doi.org/10.1080/10408348908048815

44. Kinoshita E, Ingman F, Edwall G, Thulin S, Głab S. (1986) Polycrystalline and monocrystalline antimony, iridium and palladium as electrode material for pH-sensing electrodes. Talanta 33:125–134. https://doi.org/10.1016/0039-9140(86)80028-5

45. Edwall G (1978) Improved antimony-antimony (III) oxide pH electrodes. Med Biol Eng Compu 16:661–669. https://doi.org/10.1007/BF02442445

46. Roberts EJ, Fenwick F (1928) The antimony-antimony trioxide electrode and its use as a measure of acidity. J Am Chem Soc 50:2125–2147. https://doi.org/10.1021/ja01395a010

47. Stock JT, Purdy WC, Garcia LM (1958) The antimony-antimony oxide electrode. Chem Rev 58:611–626. https://doi.org/10.1021/cr50022a001

48. Caflisch CR, Pucacco LR, Carter NW (1978) Manufacture and utilization of antimony pH electrodes. Kidney Int 14:126–141. https://doi.org/10.1038/ki.1978.100

49. Kinoshita E, Ingman F, Edwall G, Glab S (1986) An examination of the palladium/palladium oxide system and its utility for pH-sensing electrodes. Electrochim Acta 31:29–38. https://doi.org/10.1016/0013-4686(86)80057-3

50. Kim KS, Gossmann A, Winograd N (1974) X-ray photoelectron spectroscopic studies of palladium oxides and the palladium-oxygen electrode. Anal Chem 46:197–200. https://doi.org/10.1021/ac60338a037

51. Xu B, Zhang W-D (2010) Modification of vertically aligned carbon nanotubes with RuO2 for a solid-state pH sensor.

Electrochim Acta 55:2859–2864. https://doi.org/10.1016/j.electacta.2009.12.099

52. Fog A, Buck RP (1984) Electronic semiconducting oxides as pH sensors. Sensors and Actuators 5:137–146. https://doi.org/10.1016/0250-6874(84)80004-9

53. Colombo C, Kappes T, Hauser PC (2000) Coulometric microtitrator with a ruthenium dioxide pH-electrode. Anal Chim Acta 412:69–75. https://doi.org/10.1016/S0003-2670(00)00765-0

54. Kriksunov LB, Macdonald DD, Millett PJ (1994) Tungsten/tungsten oxide pH sensing electrode for high temperature aqueous environments. J Electrochem Soc 141:3002–3005. https://doi.org/10.1149/1.2059272

55. Dimitrakopoulos T, Dimitrakopoulos L, Alexander TW, Logic P, Brynn D, Hibbert D (1998) A tungsten oxide coated wire electrode used as a pH sensor in flow injection potentiometry. Anal Commun 35:395–398. https://doi.org/10.1039/A807697I

56. Cisternas R, Ballesteros L, Valenzuela ML, Kahlert H, Scholz F (2017) Decreasing the time response of calibration-free pH sensors based on tungsten bronze nanocrystals. J Electroanal Chem 801:315–318. https://doi.org/10.1016/j.jelechem.2017.08.005

57. Burke LD, Mulcahy JK, Whelan DP (1984) Preparation of an oxidized iridium electrode and the variation of its potential with pH. J Electroanal Chem Interfacial Electrochem 163:117–128. https://doi.org/10.1016/S0022-0728(84)80045-5

58. Mihell JA, Atkinson JK (1998) Planar thick-film pH electrodes based on ruthenium dioxide hydrate. Sens Actuators, B Chem 48:505–511. https://doi.org/10.1016/S0925-4005(98)00090-2

59. Kreider KG, Tarlov MJ, Cline JP (1995) Sputtered thin-film pH electrodes of platinum, palladium, ruthenium, and iridium oxides. Sens Actuators, B Chem 28:167–172. https://doi.org/10.1016/0925-4005(95)01655-4

60. Avena MJ, Cámara OR, De Pauli CP (1993) Open circuit potential measurements with Ti/TiO2 electrodes. Colloids Surf 69:217–228. https://doi.org/10.1016/0166-6622(93)80003-X

61. Guerra EM, Mulato M (2014) Titanium oxide nanorods pH sensors: comparison between voltammetry and extended gate field effect transistor measurements. Mater Sci Appl 05:459–466. https://doi.org/10.4236/msa.2014.57049

62. Campos RDC, Cestarolli DT, Mulato M, Guerra EM (2015) Comparative sensibility study of WO3 ph sensor using EGFET and ciclic voltammetry. Mater Res 18:15–19. https://doi.org/10.1590/1516-1439.252513

63. Jamal M, Razeeb KM, Shao H, Islam J, Akhter I, Furukawa H, Khosla A (2019) Development of tungsten oxide nanoparticle modified carbon fibre cloth as flexible pH sensor. Sci Rep 9:4659. https://doi.org/10.1038/s41598-019-41331-w

64. Chaisiwamongkhol K, Batchelor-Mcauley C, Compton RG (2019) Optimising amperometric pH sensing in blood samples: an iridium oxide electrode for blood pH sensing. Analyst 144:1386–1393. https://doi.org/10.1039/c8an02238k

65. O'Hare D, Parker KH, Winlove CP (2006) Metal–metal oxide pH sensors for physiological application. Med Eng Phys 28:982–988. https://doi.org/10.1016/j.medengphy.2006.05.003

66. Compton RG, Batchelor-Mcauley C, ChaisiwamongkholK Vatish M, Kennedy S (2020) Method for determining human blood pH. WO/2020/217056, 29.10.2020

67. Olthuis W, Robben MAM, Bergveld P, Bos M, Van Der Linden WE (1990) pH sensor properties of electrochemically grown iridium oxide. Sens Actuators, B Chem 2:247–256. https://doi.org/10.1016/0925-4005(90)80150-x

68. Tarlov MJ, Semancik S, Kreider KG (1990) Mechanistic and response studies of iridium oxide pH sensors. Sens Actuators, B Chem 1:293–297. https://doi.org/10.1016/0925-4005(90)80218-O

69. Yao S, Wang M, Madou M (2001) A pH electrode based on melt-oxidized iridium oxide. J Electrochem Soc 148:H29. https://doi.org/10.1149/1.1353582

70. Bause S, Decker M, Gerlach F, Näther J, Köster F, Neubauer P, Vonau W (2018) Development of an iridium-based pH sensor for bioanalytical applications. J Solid State Electrochem 22:51–60. https://doi.org/10.1007/s10008-017-3721-1

71. Dautremont-Smith WC (1982) Transition metal oxide electrochromic materials and displays: a review: part 2: oxides with anodic coloration. Displays 3:67–80. https://doi.org/10.1016/0141-9382(82)90100-7

72. Lampert CM (1984) Electrochromic materials and devices for energy efficient windows. Solar Energy Materials 11:1–27. https://doi.org/10.1016/0165-1633(84)90024-8

73. Dautremont-Smith WC, Beni G, Schiavone LM, Shay JL (1979) Solid-state electrochromic cell with anodic iridium oxide film electrodes. Appl Phys Lett 35:565–567. https://doi.org/10.1063/1.91181

74. Lauks I, Yuen M, Dietz T (1983) Electrically free-standing IrOitx thin film electrodes for high temprature, corrosive environment pH sensing. Sensors and Actuators 4:375–379. https://doi.org/10.1016/0250-6874(83)85047-1

75. Conway B, Mozota J (1983) Surface and bulk processes at oxidized iridium electrodes—II. Conductivity-switched behaviour of thick oxide films. Electrochim Acta 28:9–16

76. Mozota J, Conway B (1981) Modification of apparent electrocatalysis for anodic chlorine evolution on electrochemically conditioned oxide films at iridium anodes. J Electrochem Soc 128:2142–2149. https://doi.org/10.1149/1.2127205

77. Siracusano S, Baglio V, Grigoriev SA, Merlo L, Fateev VN, Aricò AS (2017) The influence of iridium chemical oxidation state on the performance and durability of oxygen evolution catalysts in PEM electrolysis. J Power Sources 366:105–114. https://doi.org/10.1016/j.jpowsour.2017.09.020

78. Pfeifer V, Jones TE, Velasco VJJ, Massue C, Greiner MT, Arrigo R, Teschner D, Girgsdies F, Scherzer M, Allan J, Hashagen M, Weinberg G, Piccinin S, Havecker M, Knop-Gericke A, Schlogl R (2016) The electronic structure of iridium oxide electrodes active in water splitting. Phys Chem Chem Phys 18:2292–2296. https://doi.org/10.1039/c5cp06997a

79. Pfeifer V, Jones TE, Velasco VJJ, Arrigo R, Piccinin S, Havecker M, Knop-Gericke A, Schlogl R (2017) In situ observation of reactive oxygen species forming on oxygen-evolving iridium surfaces. Chem Sci 8:2143–2149. https://doi.org/10.1039/c6sc04622c

80. Baur JE, Spaine TW (1998) Electrochemical deposition of iridium (IV) oxide from alkaline solutions of iridium (III) oxide. J Electroanal Chem 443:208–216. https://doi.org/10.1016/S0022-0728(97)00532-9

81. Salimi A, Hyde ME, Banks CE, Compton RG (2004) Boron doped diamond electrode modified with iridium oxide for amperometic detection of ultra trace amounts of arsenic (III). Analyst 129:9–14. https://doi.org/10.1039/B312285A

82. Katsube T, Lauks IR, van der Spiegel J, Zemel JN (1983) High temperature and high pressure pH sensors with sputtered iridium oxide films. Jpn J Appl Phys 22:469. https://doi.org/10.7567/jjaps.22s1.469

83. Hitchman ML, Ramanathan S (1991) Potentiometric determination of proton activities in solutions containing hydrofluoric acid using thermally oxidized iridium electrodes. Analyst 116:1131–1133. https://doi.org/10.1039/AN9911601131

84. Pickup PG, Birss VI (1988) The electrochemistry of iridium oxide films in some nonaqueous solvents. J Electrochem Soc 135:41

85. Kim TY, Yang S (2014) Fabrication method and characterization of electrodeposited and heat-treated iridium oxide films for pH sensing. Sens Actuators, B Chem 196:31–38. https://doi.org/10.1016/j.snb.2014.02.004

86. Nguyen C, Rao S, Yang X, Dubey S, Mays J, Cao H, Chiao J-C (2015) Sol-gel deposition of iridium oxide for biomedical micro-devices. Sensors 15:4212–4228. https://doi.org/10.3390/s150204212

87. Huang W-D, Cao H, Deb S, Chiao M, Chiao JC (2011) A flexible pH sensor based on the iridium oxide sensing film. Sens Actuators, A 169:1–11. https://doi.org/10.1016/j.sna.2011.05.016

88. Kuo L, Chou Y, Chen K, Lu C, Chao S (2014) A precise pH microsensor using RF-sputtering IrO2 and Ta2O5 films on Pt-electrode. Sens Actuators, B Chem 193:687–691. https://doi.org/10.1016/j.snb.2013.11.109

89. Wang M, Yao S, Madou M (2002) A long-term stable iridium oxide pH electrode. Sens Actuators, B Chem 81:313–315. https://doi.org/10.1016/S0925-4005(01)00972-8

90. Chen X, He C, Du C, Li X, Wu M (2011) Effect of heat treatment conditions on IrO2-pH electrode properties. J Univ Sci Technol Beijing 33:200–204

91. Pfeifer V, Jones TE, Velasco VJJ, Massué C, Arrigo R, Teschner D, Girgsdies F, Scherzer M, Greiner MT, Allan J, Hashagen M, Weinberg G, Piccinin S, Hävecker M, Knop-Gericke A, Schlögl R (2016) The electronic structure of iridium and its oxides. Surf Interface Anal 48:261–273. https://doi.org/10.1002/sia.5895

92. Pickup PG, Birss VI (1987) A model for anodic hydrous oxide growth at iridium. J Electroanal Chem Interfacial Electrochem 220:83–100. https://doi.org/10.1016/0022-0728(87)88006-3

93. Burke LD, Whelan DP (1984) A voltammetric investigation of the charge storage reactions of hydrous iridium oxide layers. J Electroanal Chem Interfacial Electrochem 162:121–141. https://doi.org/10.1016/s0022-0728(84)80159-x

94. Burke LD, O'Sullivan EJ (1978) Enhanced oxide growth at a rhodium surface in base under potential cycling conditions. J Electroanal Chem Interfacial Electrochem 93:11–18. https://doi.org/10.1016/S0022-0728(78)80234-4

95. Hadzi-Jordanov S, Angerstein-Kozlowska H, Vukovic M, Conway B (1977) The state of electrodeposited hydrogen at ruthenium electrodes. J Phys Chem 81:2271–2279. https://doi.org/10.1021/j100539a016

96. Colom F, Gonzalez JH, Peinado J (1978) Anodic film formation on osmium electrodes in strong acid solutions: I. Voltammetric studies. J Electroanal Chem Interfacial Electrochem 89:397–406. https://doi.org/10.1016/S0022-0728(78)80201-0

97. Burke L, Whelan D (1982) Enhanced oxide growth on tungsten in acid under potential cycling conditions. J Electroanal Chem Interfacial Electrochem 135:55–65. https://doi.org/10.1016/0022-0728(82)90004-3

98. Gottesfeld S, McIntyre J (1979) Electrochromism in anodic iridium oxide films: II. pH effects on corrosion stability and the mechanism of coloration and bleaching. J. Electrochem Soc 126:742. https://doi.org/10.1149/1.2129131

99. Hitchman ML, Ramanathan S (1988) Evaluation of iridium oxide electrodes formed by potential cycling as pH probes. Analyst 113:35–39

100. Peuckert M (1984) XPS study on thermally and electrochemically prepared oxidic adlayers on iridium. Surf Sci 144:451–464. https://doi.org/10.1016/0039-6028(84)90111-0

101. Taylor JL, Ibbotson DE, Weinberg WH (1979) The chemisorption of oxygen on the (110) surface of iridium*. Surf Sci 79:349–384. https://doi.org/10.1016/0039-6028(79)90295-4

102. Dubouis N, Grimaud A (2019) The hydrogen evolution reaction: from material to interfacial descriptors. Chem Sci 10:9165–9181. https://doi.org/10.1039/c9sc03831k

103. Jerkiewicz G (2010) Electrochemical hydrogen adsorption and absorption. Part 1: under-potential deposition of hydrogen. Electrocatalysis 1:179–199. https://doi.org/10.1007/s12678-010-0022-1

104. Jerkiewicz G, Vatankhah G, Lessard J, Soriaga MP, Park Y-S (2004) Surface-oxide growth at platinum electrodes in aqueous H2SO4: reexamination of its mechanism through combined cyclic-voltammetry, electrochemical quartz-crystal nanobalance, and Auger electron spectroscopy measurements. Electrochim Acta 49:1451–1459. https://doi.org/10.1016/j.electacta.2003.11.008

105. Burke LD, Lyons ME, O'Sullivan EJM, Whelan DP (1981) Influence of hydrolysis on the redox behaviour of hydrous oxide films. J Electroanal Chem Interfacial Electrochem 122:403–407. https://doi.org/10.1016/S0022-0728(81)80176-3

106. Carroll S, Baldwin RP (2010) Self-calibrating microfabricated iridium oxide pH electrode array for remote monitoring. Anal Chem 82:878–885. https://doi.org/10.1021/ac9020374

107. Angerstein-Kozlowska H, Conway BE, Sharp WBA (1973) The real condition of electrochemically oxidized platinum surfaces: Part I. Resolution of component processes. J Electroanal Chem Interfacial Electrochem 43:9–36. https://doi.org/10.1016/S0022-0728(73)80307-9

108. Efron B, Tibshirani R (1985) The bootstrap method for assessing statistical accuracy. Behaviormetrika 12:1–35. https://doi.org/10.2333/bhmk.12.17_1